Steel and Composite Structures, *Vol. 32, No. 3 (2019) 373-388*
DOI: https://doi.org/10.12989/scs.2019.32.3.373

Pilot study for investigating the inelastic response of a new axial smart damper combined with friction devices

Nadia M. Mirzai [1,2a] and Jong Wan Hu [*3,4]

[1] *School of Civil Engineering, College of Engineering, University of Tehran, Tehran, Iran*
[2] *Institute of Research and Development, Duy Tan University, Da Nang 550000, Vietnam*
[3] *Department of Civil and Environmental Engineering, Incheon National University, Incheon 22012, South Korea*
[4] *Incheon Disaster Prevention Research Center, Incheon National University, Incheon 22012, South Korea*

(*Received March 11, 2019, Revised June 20, 2019, Accepted July 21, 2019*)

Abstract. This study proposes a new concept of an axial damper using the combination of shape memory alloy (SMA), friction devices, and polyurethane springs. Although there are many kinds of dampers to limit the damages, large residual deformation may happen and it causes much repairing cost for restoring the structure to the initial position. Also in some of the dampers, a special technology for assembling and fabricating is needed. One of the most important advantages of this damper is the ability to remove all the residual deformation using SMA plates and simple assembling without any special technology to fabricate. In this paper, four different dampers (in presence or omission of friction devices and polyurethane springs) are investigated. All four cases are analyzed in ABAQUS platform under cyclic loadings. In addition, the SMA plates are replaced by steel ones in four cases, and the results are compared to the SMA dampers. The results show that the axial polyurethane friction (APF) damper could decrease the residual deformation effectively. Also, the damper capacity and dissipated energy could be improved. The analysis showed that APF damper is a good recentering damper with a large amount of energy dissipation and capacity, among others.

Keywords: smart material; shape memory alloy (SMA); damper; residual deformation; finite element analysis

1. Introduction

In a structure under moderate or strong earthquakes, many hinges form in the various elements, which cause deformations and damage in the structure that sometimes lead to collapse. Also, some of the existing structures that have been built according to the old codes or without appropriate seismic design at the construction time need to be retrofitted or repaired (Farzampour and Eatherton 2019, Gao *et al*. 2016, Mirtaheri *et al*. 2017). Many researchers have studied the different methods to decrease repair costs after an earthquake event. One of these methods is using different kinds of dampers to localize the damage to specific parts, which concentrates all the damage in the damper while helping the other elements of the structure to remain elastic (Azariani *et al*. 2018, Preciado *et al*. 2018, Zahrai 2015, Zahrai *et al*. 2015, Zeynali *et al*. 2018).

Thus, not only replacing this part is so fast but also the repairing cost will decrease efficiency. Although many different kinds of dampers have been developed, due to large deformation and residual interstory drift, repairing and retrofitting the structure is often not affordable. Therefore, researchers are experimenting with smart dampers and self-centering devices to omit permanent deformations. Over the past decade, shape memory alloys (SMAs) have drawn considerable attention in the civil engineering field due to their unique stress-strain behavior (Alam *et al*. 2007, DesRoches *et al*. 2004, Elbahy and Youssef 2019, Fang *et al*. 2019, Farmani and Ghassemieh 2016, Pan *et al*. 2019, Silwal *et al*. 2018, Wang *et al*. 2019, Xu *et al*. 2019, Zareie *et al*. 2017, Zheng and Dong 2019).

In addition to energy dissipation, SMAs have a special ability to recover their initial shape. They exhibit two different behaviors, the superelastic and shape memory effect (Speicher *et al*. 2011, 2017, Sultana and Youssef 2016) induced by the phase transformations of SMA. The superelastic transformation is stress induced. At a temperature above the austenite finish temperature, when an external load is applied to an SMA, the martensite phase is started: with a small increase in stress, the strain is increased significantly. After unloading, because the martensite phase is stable at higher stresses and lower temperature, the phase transformation happens, and the martensite phase is transferred to the austenite phase and makes a flag-shape curve. This flag-shape behavior is called superelastic behavior.

The shape memory transformation is temperature induced. At a temperature less than the martensite finish temperature, if loading and unloading are applied to the SMA, a large deformation remains. However, after heating the SMA above the austenite finish temperature, all the residual deformations are removed, and the material returns to its initial shape. This behavior is called the shape

*Corresponding author, Associate Professor,
E-mail: jongp24@inu.ac.kr
[a] Ph.D.

ISSN: 1229-9367 (Print), 1598-6233 (Online)

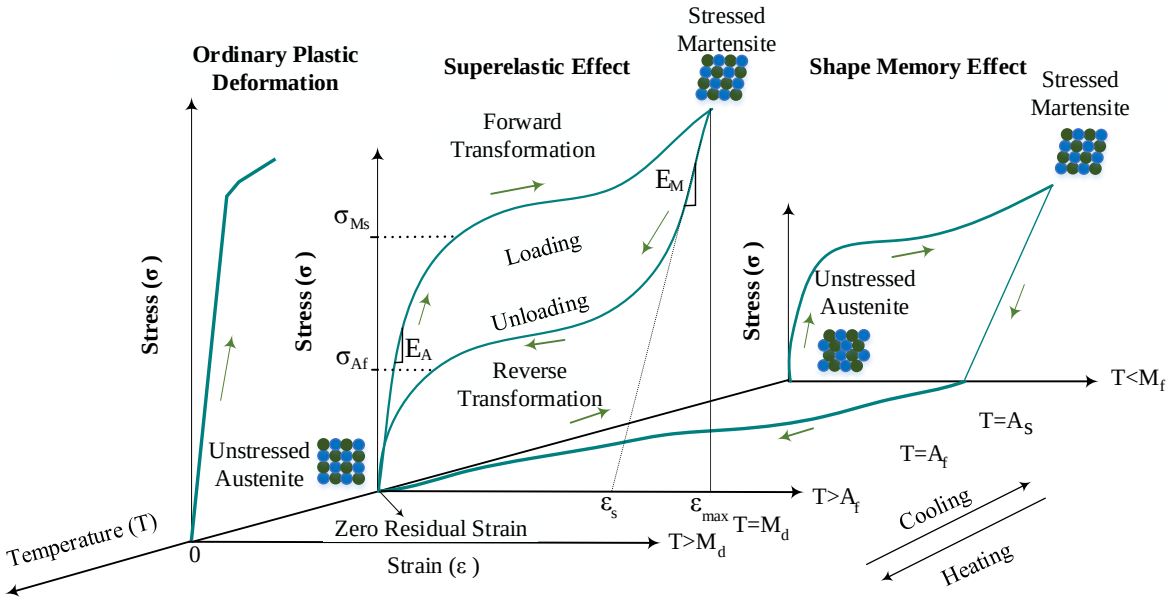

Fig. 1 Ideal stress and strain curves for superelastic SMA material (Seo *et al*. 2015)

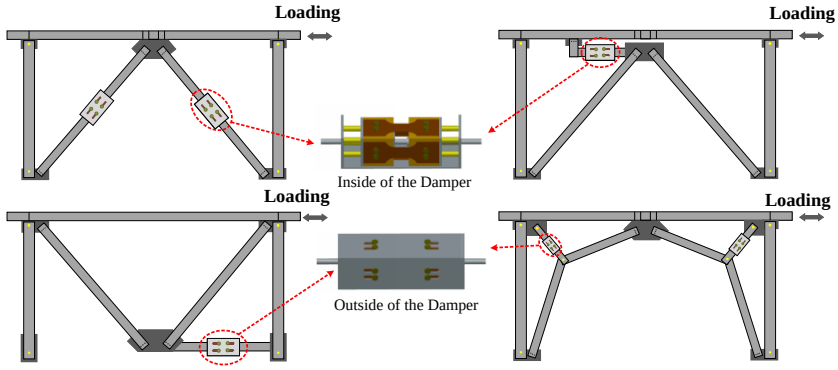

Fig. 2 Proposed recentering axial damper installed at the concentrically braced frame (CBF)

memory effect (Gao *et al*. 2016, Mirzaeifar *et al*. 2011). Fig. 1 shows SMA behavior in which E_A, E_M, σ_{Ms}, σ_{Af}, ε_s, ε_{max} refer to Young's modulus in austenite phase, Young's modulus in the martensite phase, the martensite start stress, the austenite finish stress, the maximum superelastic strain, and maximum applied strain, respectively.

Several studies have investigated employing SMAs to dampers (Kari *et al*. 2011, Mirzai *et al*. 2018, Moradi and Alam 2015). The purpose of these devices is to develop a design and installation configuration that reduces residual deformations after a seismic event (Ozbulut and Hurlebaus 2011, Zareie *et al*. 2019a, b).

In this study, superelastic nickel-titanium (NiTi) SMA is employed in a new recentering axial damper equipped with friction devices and polyurethane springs. Except for the SMA plates and polyurethane springs, which are a kind of polymer and work under pressure loads, the other parts of the damper are steel plates. Since the assembling and constructing of the damper does not need high technology, it is cheap to fabricate. In this damper, the SMA plates play the role of a self-centering system and eliminate all the residual deformations. To understand the behavior of individual components, the axial damper is studied in the absence of friction devices and polyurethane springs. All four cases are investigated using ABAQUS, which is a powerful finite element software to study micro models. Furthermore, the SMA plates are replaced by steel plates in all cases to compare the steel to the SMA dampers.

2. Model design

The axial polyurethane friction (APF) damper is a passive control device equipped with friction devices and polyurethane springs. Dog-bone SMA plates are primarily employed to achieve a recentering capability. In addition to the recentering behavior of SMA, the superelastic effect dissipates energy. The friction forces are provided by eight bolts at each side of the damper whereby the friction between the bolts and holes produces the friction forces, which enhance the energy dissipation. Furthermore, the polyurethane springs increase the ultimate capacity of the damper and increase the recentering ability. The proposed damper can be installed in all kinds of bracing systems as

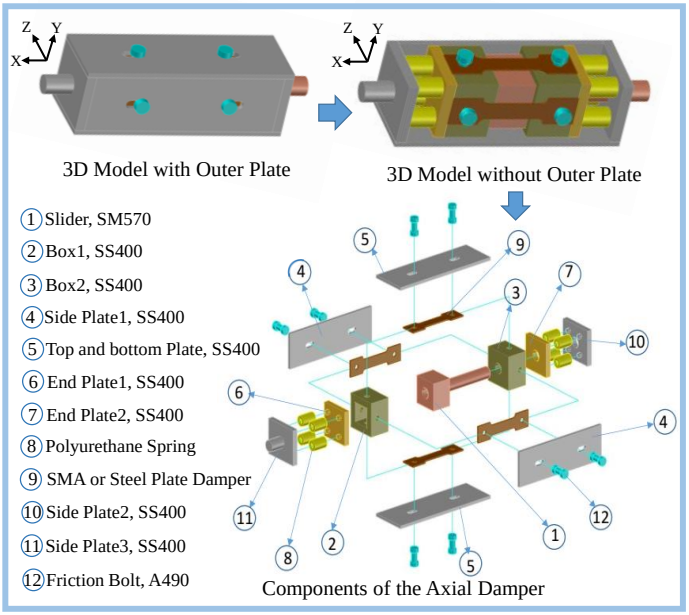

Fig. 3 3D schematic drawing of the axial damper components

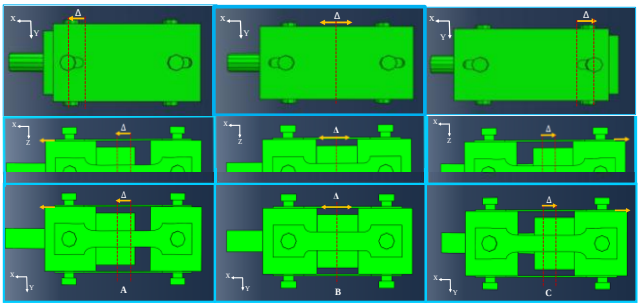

Fig. 4 Movement of the axial damper system under cyclic displacement loading (Deformation magnification factor = 3)

well as useing in rehabilitation of the structures. Fig. 2 shows the APF in different bracing systems.

Fig. 3 illustrates all components of the APF damper proposed in this study. The outer plates (No. 4, 5, 10 and 11) play the role of the friction devices as well as the cover plates. The friction coefficient is considered 0.3. The green boxes (No. 2 and 3) are movable, and the dog-bone SMA plates (No. 9) are screwed to them using the friction bolts (No. 12). The end plates (No. 6 and 7) are fixed to the green boxes, and the polyurethane springs are installed on them. The damper is connected to the main structure using two bars so that one is fixed and the other is the slider handle. As can be seen in Fig. 4, the APF damper can operate in both tension and pressure loads.

When loading is applied to the APF damper, the slider (No. 1) is moved to the right and left directions. As it moves towards the right direction, it pulls Box1 (No. 2).

Simultaneously, due to the position of the bolts in the friction holes (see the 3D model with outer plates), Box 2 (No. 3) cannot be moved. Therefore, the SMA plates are subjected to tensile forces, as well as frictional forces produced by the right friction bolts. Also, the right

Table 1 ID and definition for all axial damper models

Model ID	Definition
A-SMA	Axial SMA damper without polyurethane springs and friction devices
AP-SMA	Axial SMA damper including polyurethane springs
AF-SMA	Axial SMA damper including friction devices
APF-SMA	Axial SMA damper including polyurethane springs and friction devices
A-Steel	Axial steel damper without polyurethane springs and friction devices
AP-Steel	Axial steel damper including polyurethane springs
AF-Steel	Axial steel damper including friction devices
APF-Steel	Axial steel damper including polyurethane springs and friction devices

polyurethane springs are under pressure. Sincethe APF damper is a symmetric damper, a similar behavior occurs in the other direction. Fig. 4 illustrates the deformed shape of the axial recentering damper.

To investigate the effect of each component of the APF damper, eight cases are considered. Table 1 represents the ID of each case. To understand the influence of SMA plates on the recentering axial damper, the SMA dog-bone plates are replaced by steel ones. The “SMA” and “steel” labels of the model ID refer to the SMA dog-bone plates and steel ones, respectively.

3. Response mechanism

In the APF damper, the SMA or steel plates, friction devices, and polyurethane springs behave in parallel, and the total behavior is under the influence of the individual

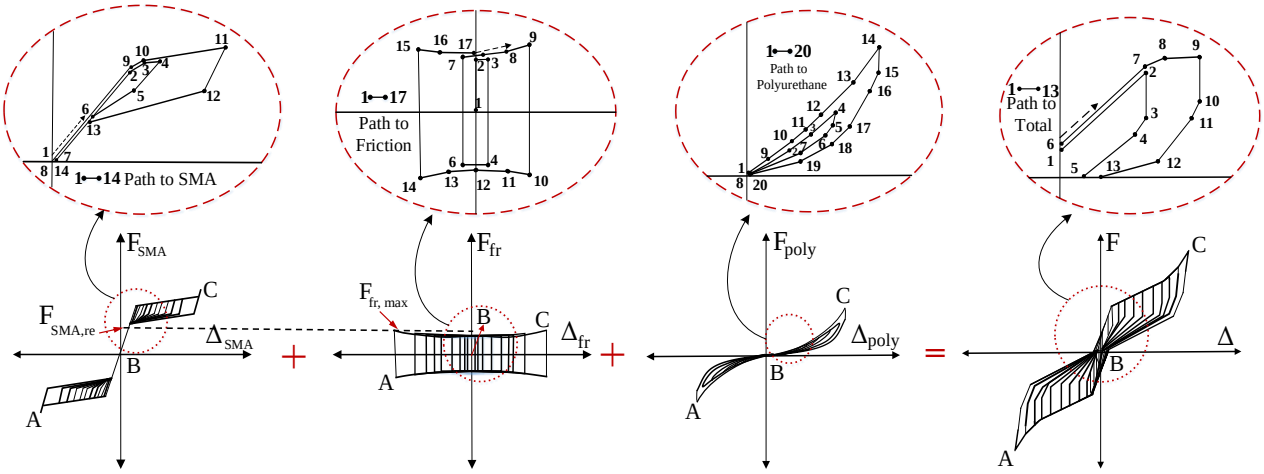

a) Behavior of the SMA Plate Damper b) Behavior of the Friction Device c) Behavior of the Polyurethane Spring d) Total Behavior of the Damper

Fig. 5 Response mechanism of the recentering axial SMA damper (APF-SMA model)

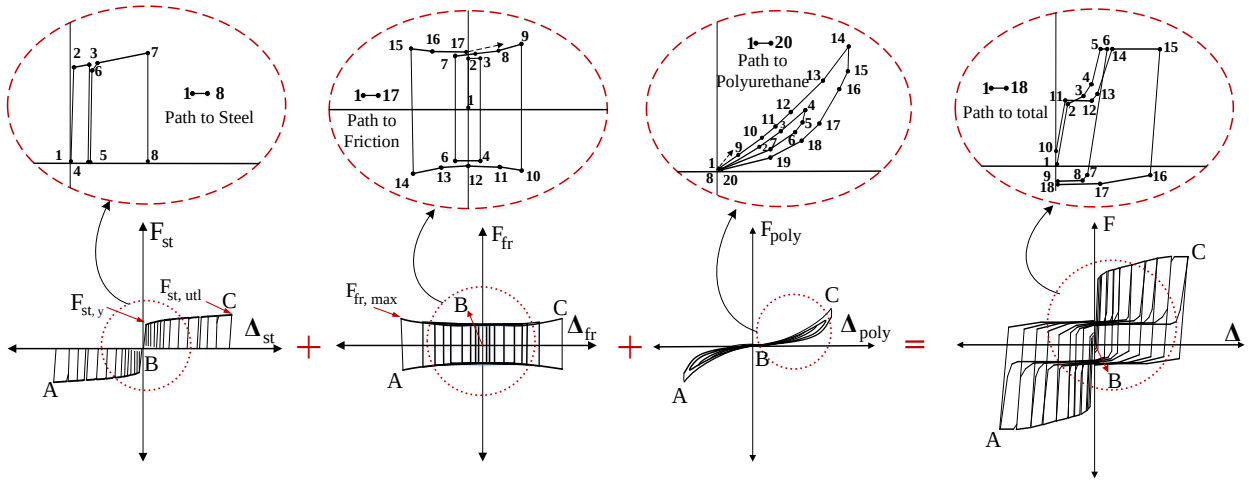

a) Behavior of the Steel Plate Damper b) Behavior of the Friction Device c) Behavior of the Polyurethane Spring d) Total Behavior of the Damper

Fig. 6 Response mechanism of the axial steel damper (APF-Steel model)

components. Therefore, it is essential to investigate the relationship between the components and total behavior. Fig. 5 shows the response mechanism of the APF-SMA damper based on theoretical observations. Where *FSMA*,*re* and *Ffr*,*max* refer to the SMA recentering force (austenite finish force) and maximum friction force, respectively.

The SMA plate damper is characterized by a flag-shaped curve. The friction device is defined by a rectangular stable curve. When a load is applied to the slider, the friction bolts start to move abruptly. Therefore, the initial stiffness is high, and the movement is similar to that of the slipping. The behavior of the polyurethane springs can be represented by a nonlinear recentering curve that affects the total stiffness.

FSMA, *re* which refers to the austenite finish force, is an important parameter in the design of the other components of the damper. According to the thickness of the alloy, this parameter changes (DesRoches *et al*. 2004). Eq. (1) presents the force ratio (*FR*), which is the portion of *Ffr*, *max* divided by *FSMA*, *re*. The maximum friction force should be close to the *FSMA*, *re* to achieve optimum total behavior with small residual deformation and maximum energy dissipation. The ratios close to 100% are the best cases, and by mitigating the *FR* ratio, the energy dissipation is decreased. For the ratios higher than 100%, the recentering will decrease, and more permanent deformation is expected. In a structure, to achieve the maximum *FR*, which is related to the austenite finish force, and maximum friction force, the SMA plates should be designed first, such that the length of the SMA plates are defined based on the maximum displacement of the slider while the thickness of the plates is determined according to the residual drift. After finalizing the dimensions of the SMA plates, the maximum friction and polyurethane springs force is defined. The maximum friction force should be the same as *FSMA*, *re* to produce the minimum residual deformations in the structure. Moreover, the polyurethane springs affect the stiffness and maximum capacity of the damper. Thus, the

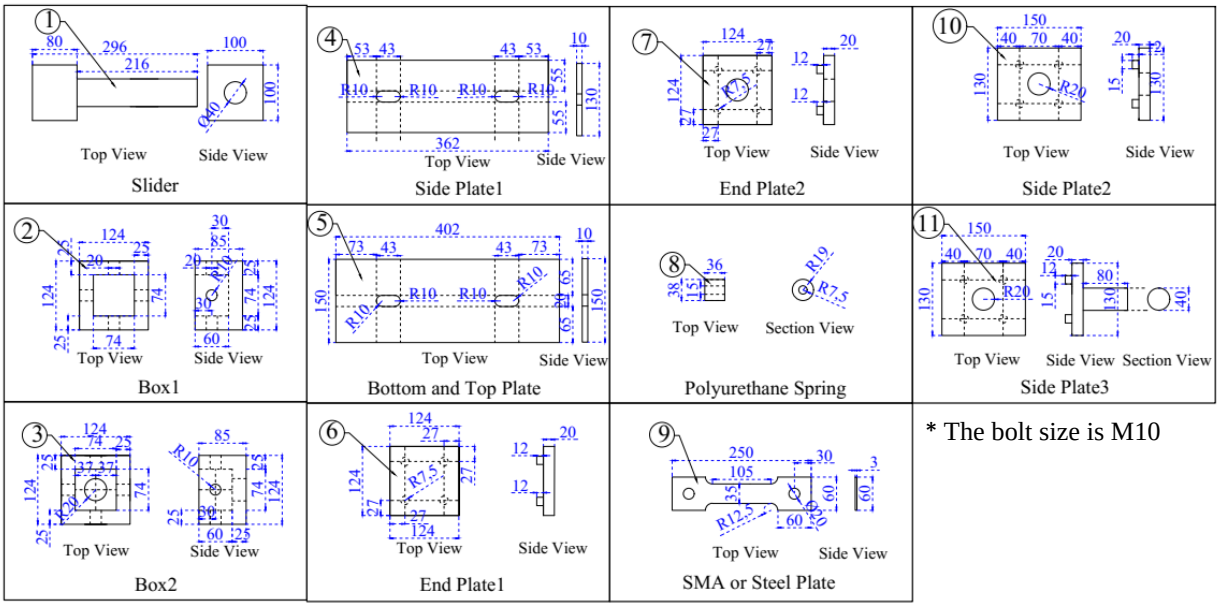

Fig. 7 Design of the recentering axial damper with the friction devices (all dimensions in mm)

stiffness of the damper should not be more than that of the other elements.

$$FR = \gamma = \frac{F_{fr,\max}}{F_{SMA,re}} \times 100 \quad or \; FR = \gamma = \frac{F_{fr,\max}}{F_{st,y}} \times 100 \tag{1}$$

The dissipation energy is the summation of the area of all the hysteretic loops. Therefore, as can be seen in Fig. 5, the dissipation energy of the total behavior has been increased significantly in comparison to that of the SMA plate damper. Fig. 6 presents the total behavior and response mechanism of the APF-Steel damper. The APF-Steel damper is not equipped with any recentering device (the effect of polyurethane springs is negligible). Therefore, there is a lot of residual deformation due to the metallic yielding. In addition, a bigger area is produced, which leads to a lot of energy dissipation in the APF-Steel model (see the total behavior).

The total behavior can define by superposition of the three forces in parallel at the same displacement as presented in Eqs. (2)-(3).

$$F = F_{SMA} + F_{fr} + F_{poly} \quad or \; F = F_{st} + F_{fr} + F_{poly} \tag{2}$$

$$\Delta = \Delta_{SMA} = \Delta_{fr} = \Delta_{poly} \quad or \; \Delta = \Delta_{st} = \Delta_{fr} = \Delta_{poly} \tag{3}$$

Where *FSMA*, *FSt*, *Ffr*, and *Fpoly* refer to the SMA plate damper force, steel force, friction force, and polyurethane springs force. Δ*SMA*, Δ*fr*, Δ*poly*, and Δ*st*

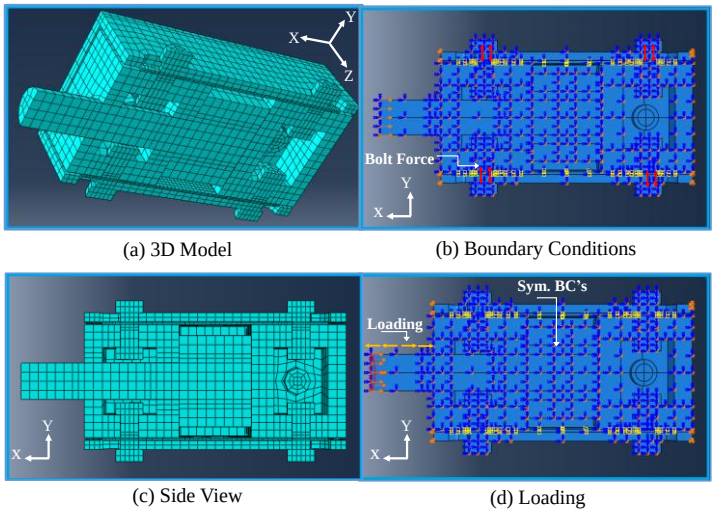

(a) 3D Model (b) Boundary Conditions

(c) Side View (d) Loading

Fig. 8 Finite element models for the axial damper models

define SMA displacement, friction displacement, polyurethane springs displacement, and steel displacement, respectively. The friction devices and polyurethane springs should be designed based on the SMA plates and *FR* ratio. In addition, the steel plates have been designed for elastic behavior. Fig. 7 shows the details of the damper's components. The finite element model also is simulated regarding the designed dimension.

4. Finite element analysis (FEA)

As the recentering axial damper is newly proposed in this research, it is essential to investigate the behavior and response under cyclic loading through refined 3D FE analysis. Eight FE models were developed for the different cases of the axial recentering damper according to Table 1. To predict the real behavior, the components of the damper are simulated using the 8-node solid 3D element and generated by mesh division to achieve sufficient accuracy and quick convergence (Fig 8(a)). Furthermore, the key elements such as SMA plates and the bolts were generated using finer meshes. Due to the effect of friction forces on the bolts and the bearing effect, the bolts are modeled in details. To apply the bolt forces, two separate loading time steps are used. The first static time step is for applying the bolts load, and after completion, the displacement-control cyclic loading is applied to the slider at the second static time step (Figs. 8(b) and (d)). To prevent rigid body movement, the bolts are fixed at the first time step and released at the second step. As the damper is symmetric, half of the damper is simulated, and the symmetric boundary conditions (BCs) are used (Fig. 8(d)). Fig. 8(c) also shows the side view of the recentering axial damper.The steel material is simulated using the combined hardening model, which includes the Bauschinger effect, stress relaxation, and ratcheting response. For steel grade SS570, the equivalent stress ($\sigma 0$), Q-infinity ($Q\infty$) and hardening parameter (b) are 450 MPa, 500 MPa and 0.12, respectively; while for the steel grade SS400 they are 255.9 MPa, 227.8 MPa and 5.8 where $\sigma 0$ is the yield stress at zero equivalent plastic strain, $Q\infty$ is the maximum variation of the size of the yield surface, and b refers to the rate where the size of the yield surface varies as the plastic strain increases. The material nonlinearity is taken into account in the individual parts. In addition, the geometric nonlinearity is considered in the FE model.

The interaction between the contacting bodies is friction with a friction coefficient of 0.3 in the tangency direction and hard contact in the normal direction. The material properties of all the steel parts, except the slider, is steel type SS400 with a yielding stress of 235 MPa, the ultimate stress of 400 MPa and an elastic modulus equal to 210 GPa. The slider material is SM570, and the yielding stress, ultimate stress, and elastic modulus are 450 MPa, 570 MPa and 210 GPa, respectively. The steel material is simulated using the combined hardening model, which includes the Bauschinger effect, stress relaxation, and ratcheting response. The material nonlinearity is taken into account in the individual parts. In addition, geometric nonlinearity is considered in the FE model.

4.1 Verification study

Since the SMA material is not in the ABAQUS library by default, the user-defined material (UMAT) model is assembled in the ABAQUS library (Auricchio and Sacco 1997). The SMA properties are according to the uniaxial pull-out test performed by (Hu *et al*. 2018). Fig. 9 shows good agreement between the experimental result and the simulation. The SMA input properties the elastic modulus, martensite start stress, and finish stress are 32 GPa, 450 MPa, and 620 MPa, respectively. The austenite finish stress is also 130 MPa, and the austenite start stress is 350 MPa. The Poisson's ratio is 0.33, the transformation reference temperature is 25℃, and transformation strain is 0.06 rad. The polyurethane spring is verified in the experimental test, which has been performed by Esko-RTS in Korea using the spring element and the multilinear material is applied to the element. Fig. 10 illustrates the agreement between the experiment and simulated model.

4.2 FE analysis results

The loading history used for the cyclic analysis is adopted from (Lu *et al*. 2017). The results are evaluated in the S1 to S5 cycles. The S5 cycle refers to the residual deformation at the damper. Fig. 11 illustrates the loading history. The maximum displacement is considered based on

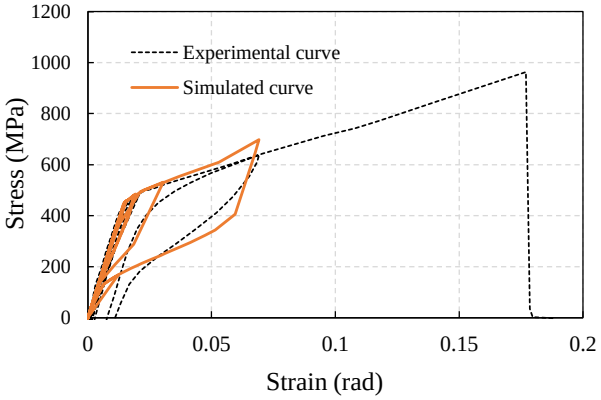

Fig. 9 Material behavior of the superelastic SMA plates

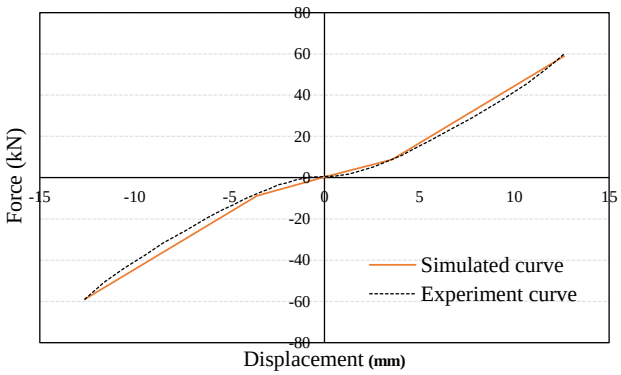

Fig. 10 Material behavior of the Polyurethane springs

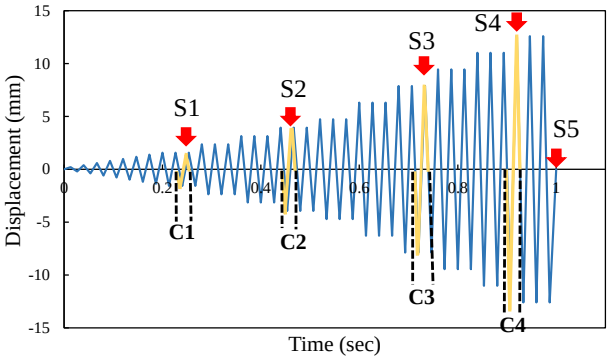

Fig. 11 Cyclic displacement loading history and measurement points (Lu *et al*. 2017)

the 12% strain (12.6 mm) at the SMA plates to ensure a failure happens.

The results obtained in the FE analysis are as follows. The cyclic displacement-control analysis is applied to the slider, and the displacement is obtained from the location of the applied load. The results represent approximate symmetric hysteresis loops under compression and tension loadings. Fig. 12 shows the total behavior of the recentering axial SMA damper.

Fig. 12(a) is the behavior of the S-SMA. The damper response is consistent with the SMA flag-shaped behavior, and the residual displacement is very small. Fig. 12(b) refers to the SP-SMA damper, including the polyurethane springs. As can be seen, the ultimate capacity and stiffness of the damper has been increased, and there is little residual displacement. The effect of friction devices is shown in Fig. 12(c). Although friction devices improve the energy dissipation by expanding the area of the hysteresis loops, they result in the degradation of the recentering ability. Fig. 12(d) is the combination of all effects. Both the energy dissipation and maximum capacity have been improved and the maximum capacity is more than in other cases. As can be seen, the residual displacement in all cases is negligible and the dampers are able to recover to their original condition.

The axial steel damper is shown in Fig. 13. In comparison to the axial SMA damper, the ultimate force (*Fult*) in the steel dampers is less than that in all the SMA cases. In spite of little residual displacement of the axial SMA damper, the residual displacement (Δ*res*) is close to the ultimate displacement (Δ*ult*) and considerable displacement has remained in the damper after unloading. Furthermore, the behavior of the axial steel damper is not symmetric. This is due tothe residual deformation and leads to small energy dissipation in compression. Therefore, contrary to the theorical relationships (Fig. 6), the energy dissipation has not been improved.

Figs. 14 and 15 represent the von-Mises stresses of the APF-SMA and APF-Steel dampers in the different loading cycles, respectively. On the basis of the figures, increasing the displacement leads to higher stresses as expected. Also, maximum stress occurs in the middle of the dog-bone plates. Fig. 14(d) shows the maximum displacement (12.6 mm), and the failure probably happens before that. The von-Mises stresses are up to 650 MPa, and the stress concentration occurs in the middle of the SMA plates. The other parts of the APF-SMA damper have small stresses. At the slider, the stresses are close to 400 MPa, which is in the

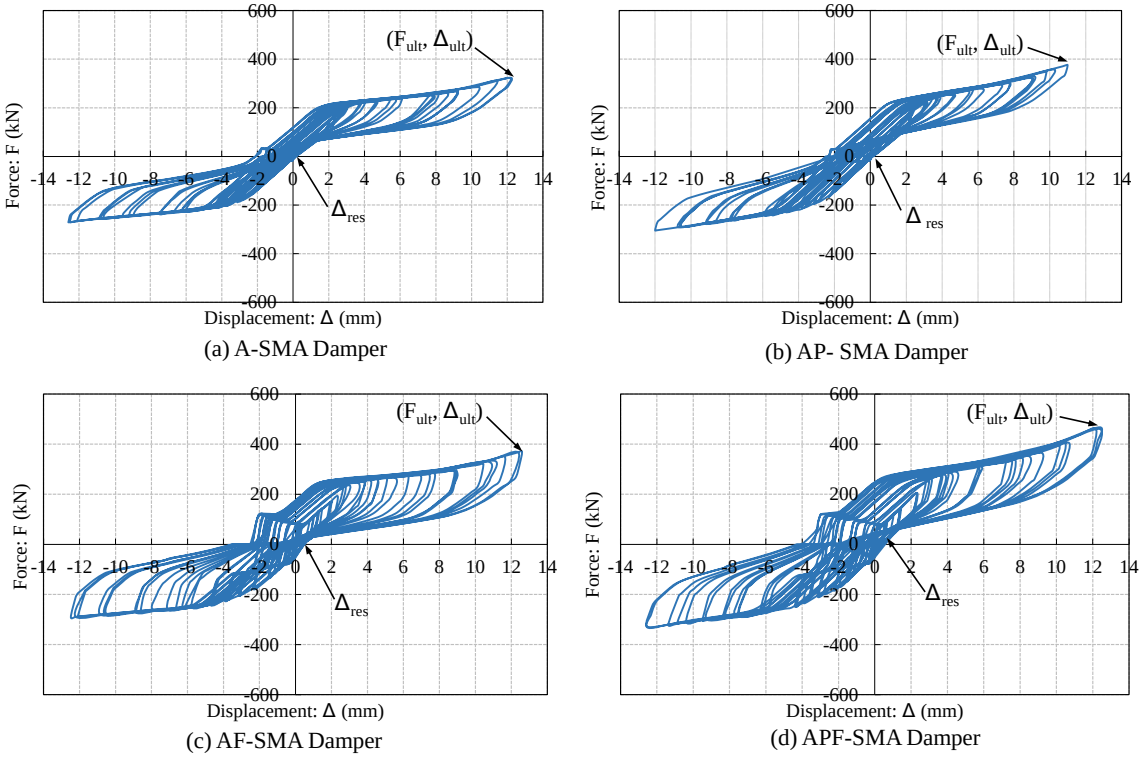

(a) A-SMA Damper

(b) AP- SMA Damper

(c) AF-SMA Damper

(d) APF-SMA Damper

Fig. 12 Total behavior of the recentering axial SMA damper models

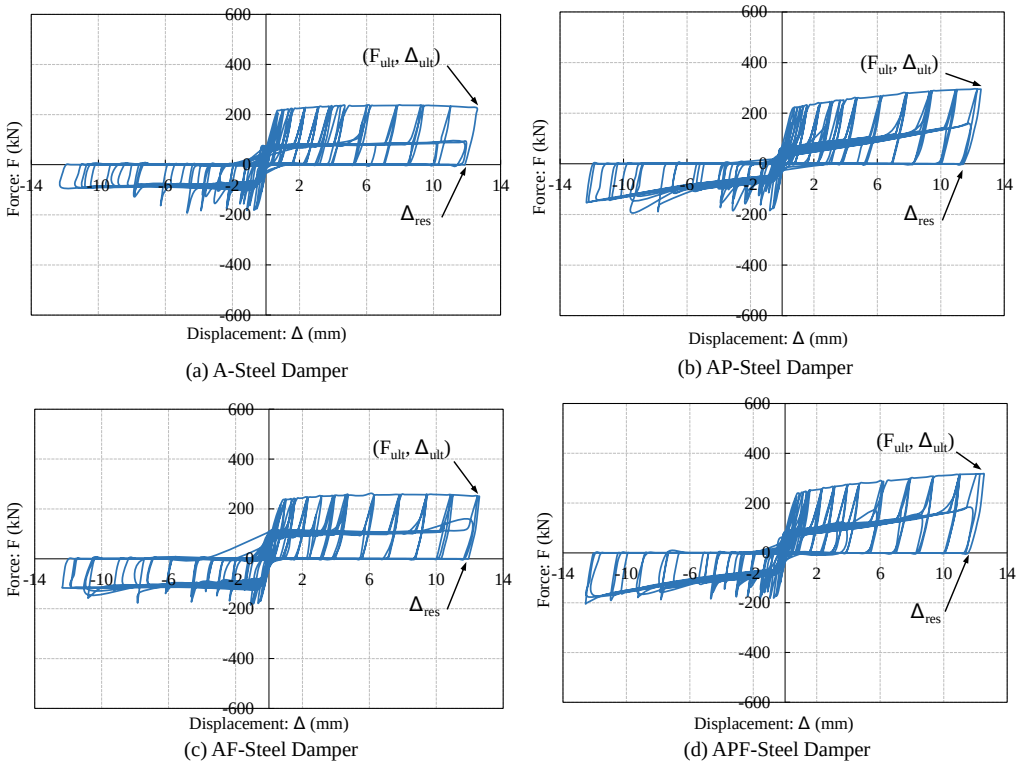

Fig. 13 Total behavior of the axial steel damper models

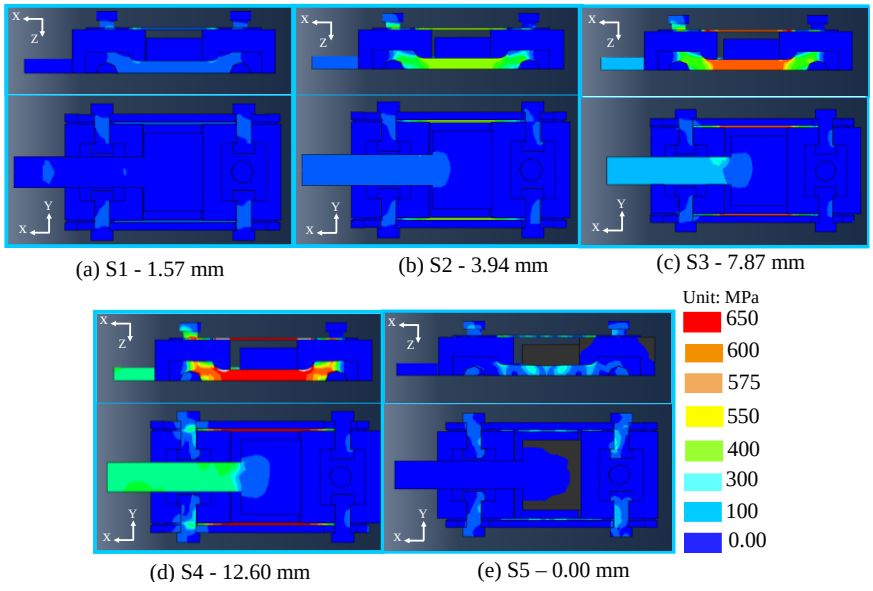

Fig. 14 von-Mises stress contours for the recentering axial SMA damper (APF-SMA model)

elastic range for SM570 steel with yielding stress of 450 MPa. Fig. 14(e) shows the von-Mises stresses after unloading (cycle S5). As can be seen in Fig. 14(e), the residual displacement is about 178 MPa and the damper has returned to the initial position. Whereas the maximum stress of the APF-Steel (Fig. 15(e)) is 400 MPa, which indicates permanent stress higher than the yielding stress of the steel plates. Therefore, the APF-Steel damper does not recover its initial shape.

As the stresses concentrate at the dog-bone plates, the axial stresses of the SMA and steel plates are compared in Figs. 16 and 17. As mentioned before, in both figures, the failure happens at the middle of the dog-bone plates. The residual axial stress in this case is related to the 12% strain, which is more than the maximum superelastic strain (6% to 7%). Therefore residual axial stress has remained in the SMA plates while it is about 400 MPa in the steel plate. In addition, the logarithmic axial strain contours are illustrated

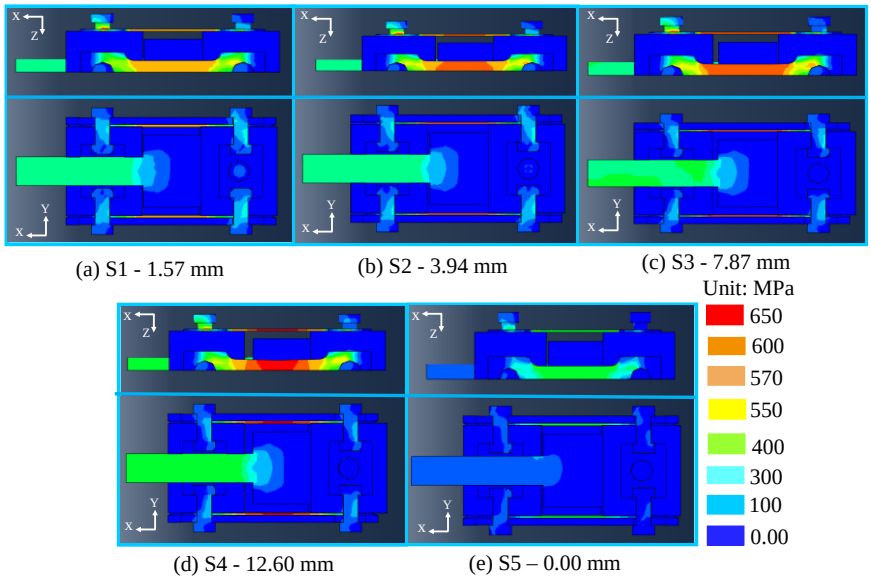

(a) S1 - 1.57 mm (b) S2 - 3.94 mm (c) S3 - 7.87 mm

(d) S4 - 12.60 mm (e) S5 – 0.00 mm

Fig. 15 von-Mises stress contours for the axial steel damper (APF-Steel model)

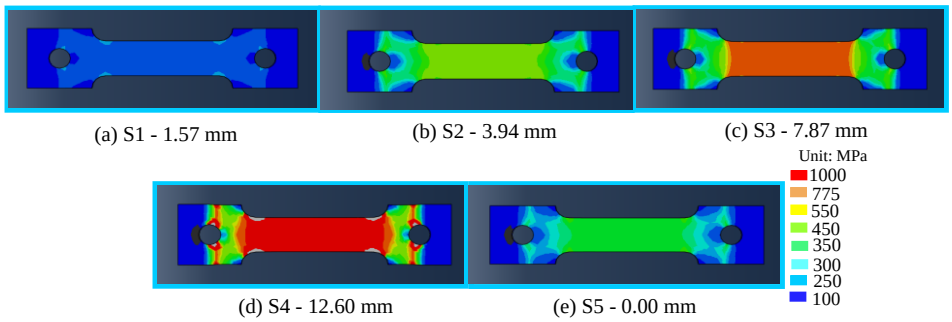

(a) S1 - 1.57 mm (b) S2 - 3.94 mm (c) S3 - 7.87 mm

(d) S4 - 12.60 mm (e) S5 - 0.00 mm

Fig. 16 Axial stress contours for the SMA plate damper in the APF-SMA model

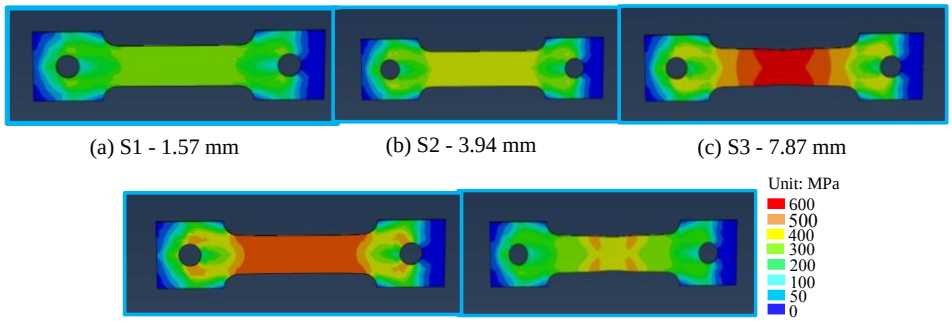

(a) S1 - 1.57 mm (b) S2 - 3.94 mm (c) S3 - 7.87 mm

(d) S4 - 12.60 mm (e) S5 - 0.00 mm

Fig. 17 Axial stress contours for the steel plate damper in the APF-Steel model

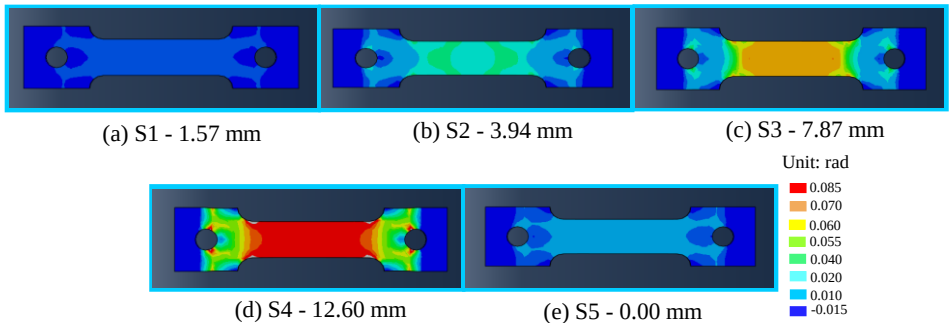

(a) S1 - 1.57 mm (b) S2 - 3.94 mm (c) S3 - 7.87 mm

(d) S4 - 12.60 mm (e) S5 - 0.00 mm

Fig. 18 Logarithmic axial strain contours for the steel plate damper in the APF-SMA model

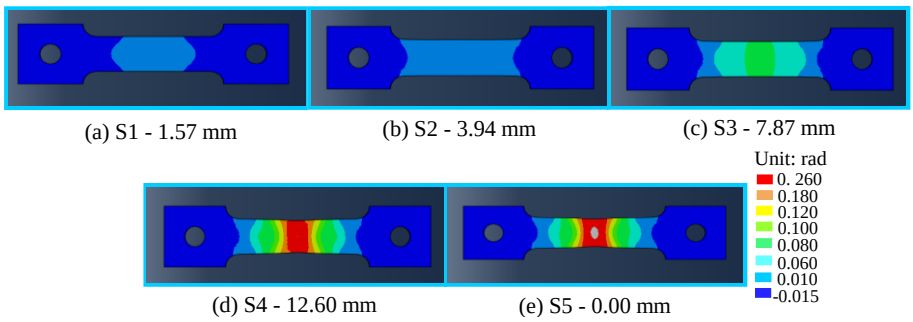

Fig. 19 Logarithmic axial strain contours for the steel plate damper in the APF-Steel model

in Figs. 18 and 19 for the SMA and steel plates, respectively. The figures confirm that the failure point is at the middle of the plates. Figs. 18(e) and 19(e) show the residual strain in the SMA and steel plates. As can be seen, there is no residual strain in the SMA plates while the residual strain is close to 0.26 rad in the steel plates.

Figs. 20 and 21 refer to the stress-strain hysteresis of the SMA and steel plates used in the axial damper. As expected, the SMA curve is flag-shaped with a maximum strain of 7%. The measurement point is in the cross section at the middle of the SMA plates. Furthermore, the results show that the obtained flag-shaped curve follows the input parameters such as the martensite start point of 450 MPa and the martensite finish point of 620 MPa. The austenite start and finish stresses are about 350 MPa and 120 MPa, respectively. Also, in Fig. 21, the loading and unloading slope is the same as the initial slope, which is an inherent characteristic of the steel. In addition, the yield stress is close to 450 MPa and the maximum strain is about 0.25 rad.

5. Observations and performance evaluation

To evaluate the effect of each component, it is important to compare the results of each component, individually. Therefore, the behavior of four recentering axial SMA dampers and axial steel dampers are investigated at the different cycles in Figs. 22 and 23. As Figs. 22(a) and (b) show, in the first cycles, there is no difference between the four cases. After several cycles in which the displacement is increased, different effects on each component appears. Figs. 22(c) and (d) show that the AP and APF are the same stiffness and ultimate strength, which is the effect of the polyurethane springs. Also, the AF and A have the same stiffness and ultimate force. These results indicate that the friction devices do not apply much stiffness to the damper.

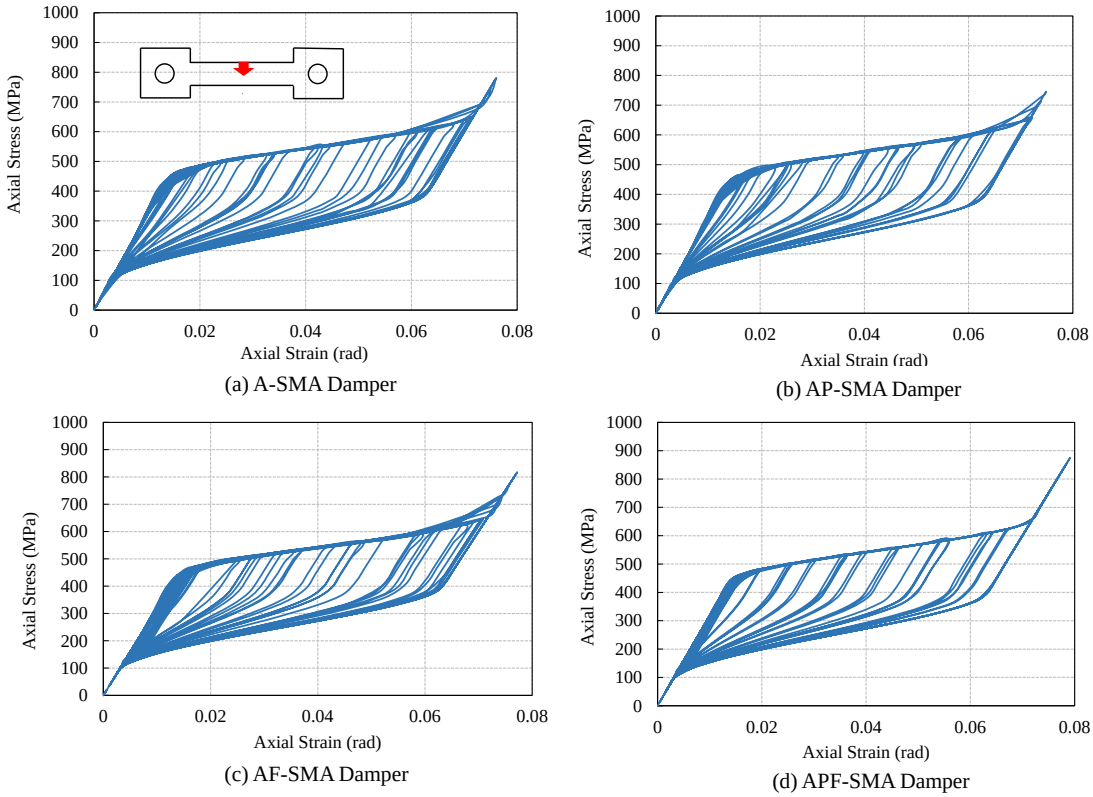

(a) A-SMA Damper

(b) AP-SMA Damper

(c) AF-SMA Damper

(d) APF-SMA Damper

Fig. 20 Stress and strain curves measured in the middle of the SMA plate dampers

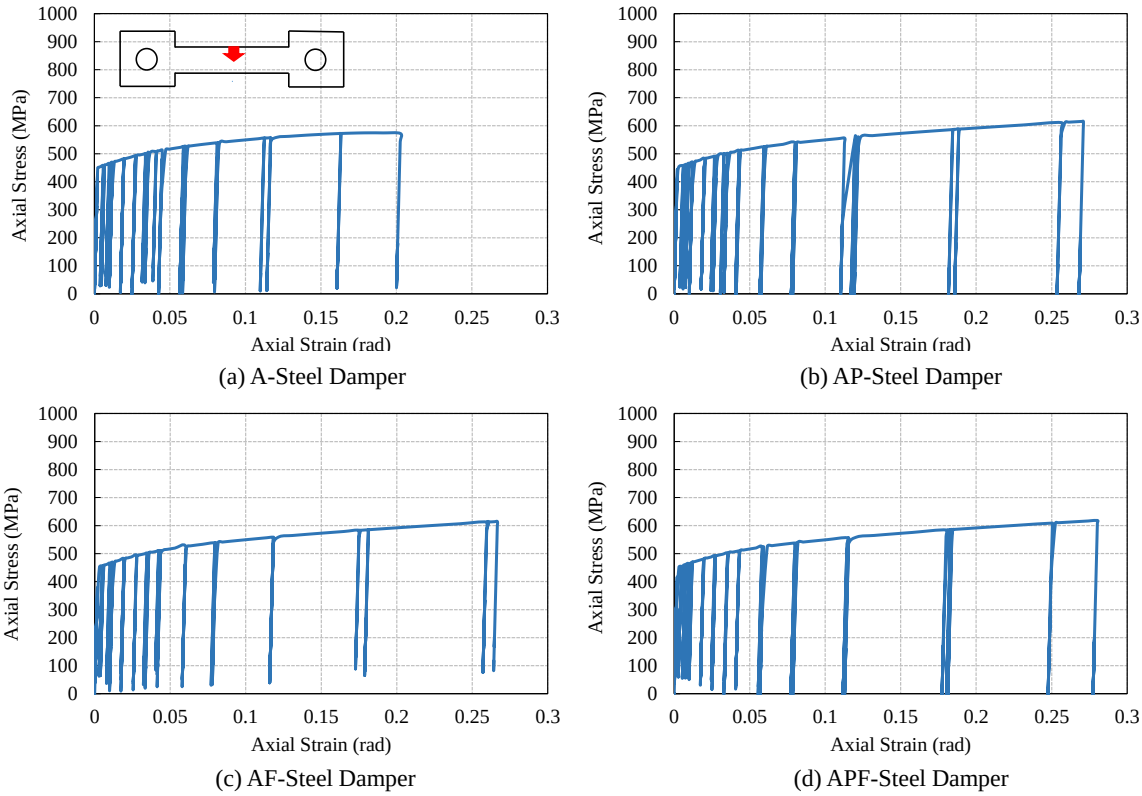

Fig. 21 Stress and strain curves measured in the middle of the steel plate dampers

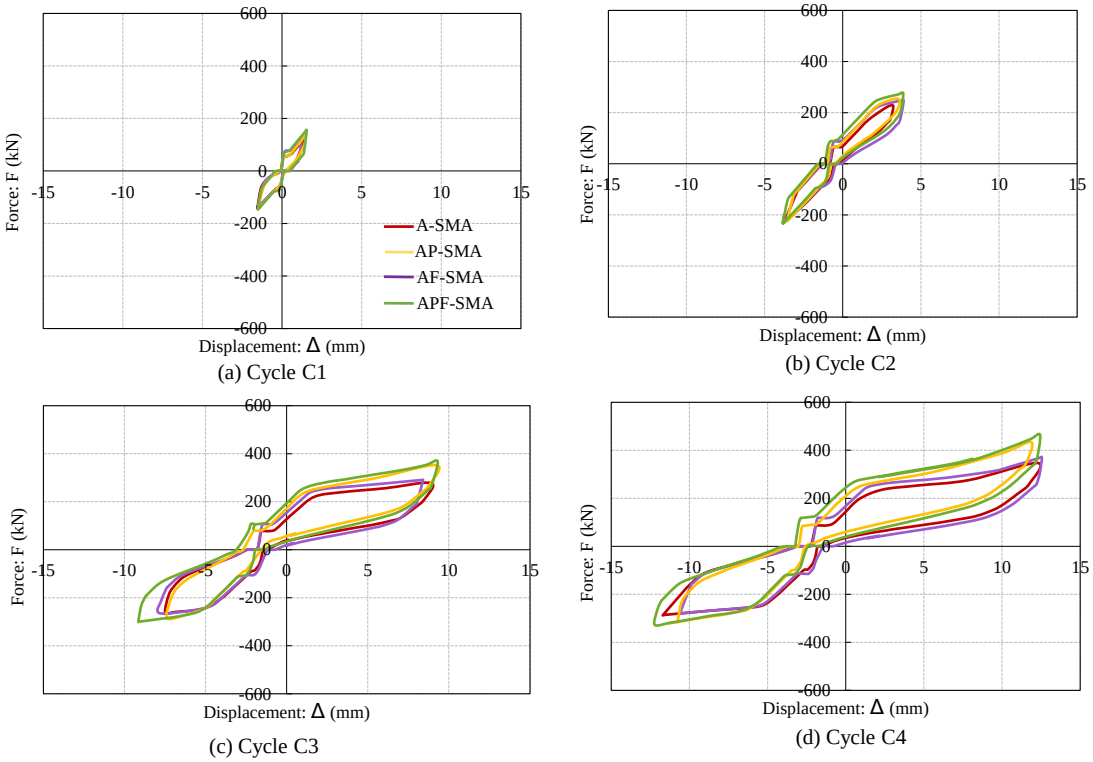

Fig. 22 Total force and displacement curves for the recentering axial SMA damper models under individual specific cycles

The area of the AF damper is more than that of A in each cycle, which shows the energy dissipating effect of the friction devices, and similarly, the area of the APF damper is more than that of the AP. In all SMA dampers, the residual displacement is very small due to the recentering capability according to the phase transformation of the SMA plates.

On the other hand in Fig. 23, the effect of the friction devices and polyurethane springs in the axial steel damper is the same as that in the SMA axial damper but in all cycles, there is some bearing tension due to the permanent deformation. Furthermore, as can be seen, the energy dissipation is less than that in the SMA axial dampers.

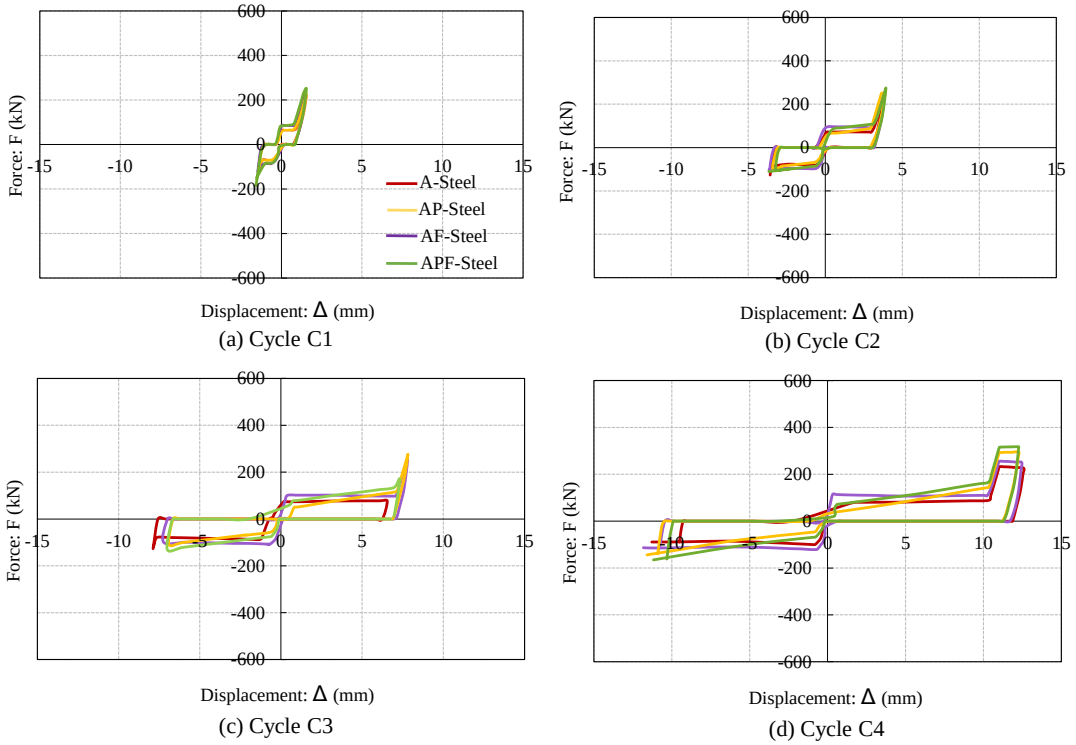

Fig. 23 Total force and displacement curves for the axial steel damper models under individual specific cycles

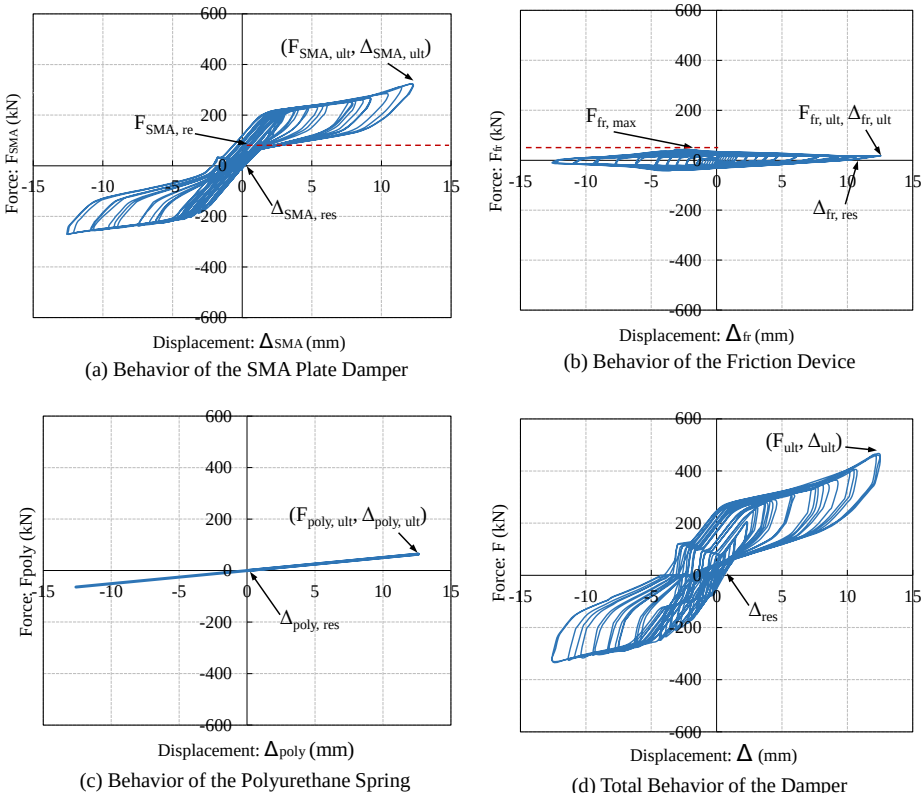

Fig. 24 Response mechanism curves for the APF-SMA model components

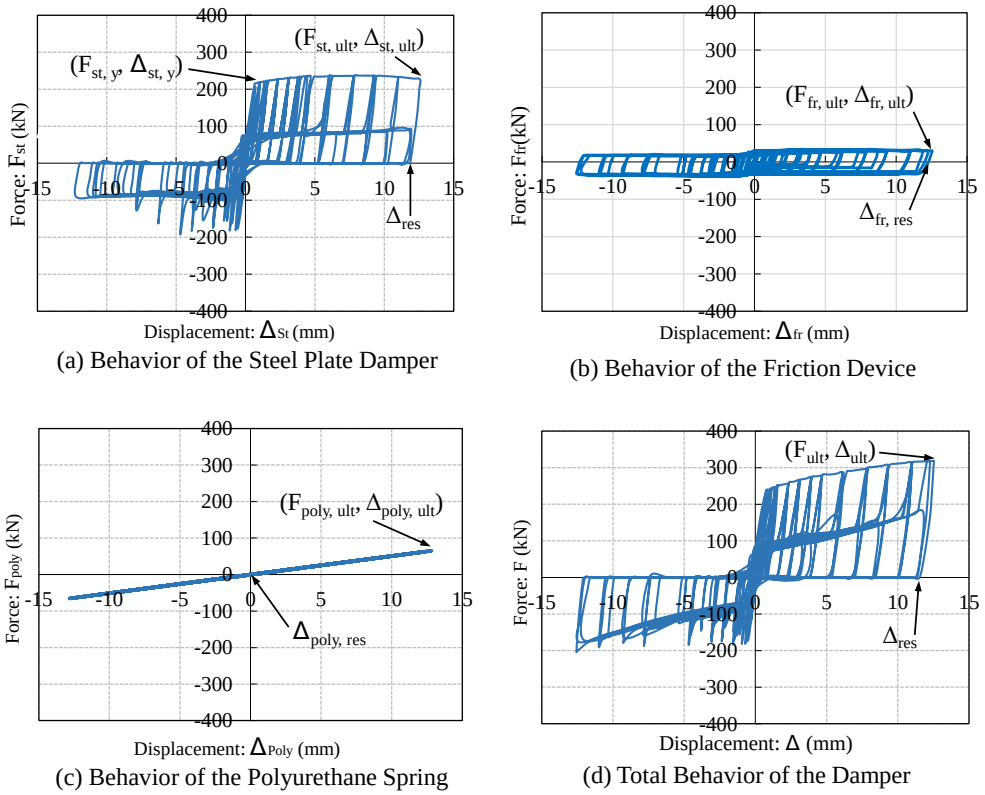

(a) Behavior of the Steel Plate Damper

(b) Behavior of the Friction Device

(c) Behavior of the Polyurethane Spring

(d) Total Behavior of the Damper

Fig. 25 Response mechanism curves for the APF-Steel model components

In addition, it is important and necessary to investigate whether or not the assembling of the individual components is compatible with the total behavior of the APF damper, and the simulation is correct. The behavior of each component obtained from ABAQUS has been shown in Fig. 24 for the APF-SMA damper and Fig. 25 for the APF-Steel damper. In these figures, $F_{SMA,ult}$, $F_{SMA,re}$, $F_{fr,ult}$, $F_{poly,ult}$, F_{ult}, $F_{st,y}$ and $F_{st,ult}$ are defined as the SMA ultimate force, SMA recentering force, ultimate friction force, ultimate polyurethane springs force, ultimate force, steel yield force and steel ultimate force, respectively. Also, $\Delta_{SMA,ult}$, $\Delta_{fr,ult}$, $\Delta_{poly,ult}$, Δ_{ult}, $\Delta_{st,y}$ and $\Delta_{st,ult}$ refer to the SMA ultimate displacement, friction devices ultimate displacement, polyurethane springs ultimate displacement, ultimate displacement, and steel yield displacement, respectively.

As can be seen in Fig. 24(a) and Fig. 24(b), the maximum friction force (*Ffr*, *max*) is close to the recentering force (*FSMA*, *re*) based on achieving the optimal design of the damper. The desirable case should have an equal quantity of the recentering and friction force. The behavior of each component shows that ABAQUS could simulate each component behavior, perfectly. Furthermore, there is a small quantity of the residual displacement in the APF-SMA due to the produced permanent deformation by the friction devices. In addition, the ultimate force of the APF-SMA is larger than that of other SMA dampers, which confirms the influence of the polyurethane springs. Also, the area of the hysteresis loops of the APF-SMA is larger than that of the other dampers, which confirms the effect of the friction devices.

The obtained results of the APF-Steel also show that the effect of the polyurethane springs is similar to that of the APF-SMA damper but there is a large quantity of residual deformation due to the absence of recentering devices in this damper. On the other hand, the effect of the friction devices is less than that in the APF-SMA damper.

The details about the specific values of each parameter of the axial SMA and steel dampers have been reported in Table 2 and Table 3, respectively. The force ratio (*FR*) is defined in Eq. (1) and the recentering ratio (*RR*) – defined as the maximum recentering displacement divided by ultimate displacement – is presented in Eq. (4). The total energy (*TE*) can be calculated by the summation of the area of the hysteresis loops. Also, the energy ratio (*ER*), which refers to the portion of the friction mechanism, is presented in Eq. (5).

$$RR = \frac{100\,(\Delta_{ult} - \Delta_{res})}{\Delta_{ult}} \tag{4}$$

$$ER = \frac{100\,(E_{fr})}{(TE - E_{fr})} \tag{5}$$

As these results show, the maximum capacity of the dampers is related to the axial recentering of SMA dampers such that the capacity of the APF-SMA damper has been increased by 37%. The residual displacement in all axial SMA dampers is very small, but there is significant residual displacement of about 91.71% in the axial steel dampers, and the recentering ratio emphasizes it. In all cases, the recentering ratio is less than 10% for the axial steel dampers

Table 2 Performance-based evaluation for SMA axial dampers

Model ID	A-SMA	AP-SMA	AF-SMA	APF-SMA
Δ_{ult}* (mm)	7.97	7.86	8.11	8.3
$F_{SMA,ult}$ (kN)	323.65	315.68	343.28	367.52
$F_{fr,ult}$ (kN)	0	0	16.97	42.82
$F_{poly,ult}$ (kN)	0	62.84	0	62.84
F_{ult}** (kN)	323.65	378.52	360.25	473.18
F_{ult}*** (kN)	323.65	376.65	371.73	467.16
$\Delta_{SMA,res}$ (mm)	0	0	0	0
$\Delta_{fr,res}$ (mm)	0	0	12.58	12.54
$\Delta_{poly,res}$ (mm)	0	0	0	0
Δ_{res} (mm)	0.14	0.14	0.59	0.43
FR (%)	0	0	61.99	61.78
RR (%)	98.24	98.22	92.73	94.82
TE**** (kN.mm)	27457.87	28524.2	50293.88	50502.76
ER (%)	0	0	40.38	41.98

* $\Delta_{ult} = \Delta_{SMA,ult} = \Delta_{fr,ult} = \Delta_{poly,ult}$ or $\Delta_{ult} = \Delta_{st,ult} = \Delta_{fr,ult} = \Delta_{poly,ult}$
** $F_{ult} = F_{SMA,ult} + F_{fr,ult} + F_{poly,ult}$ or $F_{ult} = F_{st,ult} + F_{fr,ult} + F_{poly,ult}$
*** The obtained result from the Analysis
**** Total cumulative energy

Table 3 Performance-based evaluation for steel axial dampers

Model ID	A-Steel	AP-Steel	AF-Steel	APF-Steel
Δ_{ult}* (mm)	12.59	12.54	12.58	12.54
$F_{SMA,ult}$ (kN)	237.08	258.6	257.1	259.84
$F_{fr,ult}$ (kN)	0	0	39.55	39.69
$F_{poly,ult}$ (kN)	0	63.31	0	63.31
F_{ult}** (kN)	237.08	321.91	296.65	362.84
F_{ult}*** (kN)	237.08	295.07	258.5	318.05
$\Delta_{SMA,res}$ (mm)	9.13	8.79	5.84	5.43
$\Delta_{fr,res}$ (mm)	0	0	11.9	12.3
$\Delta_{poly,res}$ (mm)	0	0	0	0
Δ_{res} (mm)	11.8	11.4	11.9	11.5
FR (%)	0	0	17.83	16.66
RR (%)	6.27	9.09	5.41	8.29
TR**** (kN.mm)	30027.21	30814.07	39230.68	38957.64
ER (%)	0	0	78.23	95.83

* $\Delta_{ult} = \Delta_{SMA,ult} = \Delta_{fr,ult} = \Delta_{poly,ult}$ or $\Delta_{ult} = \Delta_{st,ult} = \Delta_{fr,ult} = \Delta_{poly,ult}$
** $F_{ult} = F_{SMA,ult} + F_{fr,ult} + F_{poly,ult}$ or $F_{ult} = F_{st,ult} + F_{fr,ult} + F_{poly,ult}$
*** The obtained result from the Analysis
**** Total cumulative energy

while it is more than 94% in all axial SMA dampers and shows the significant recentering ability of the axial SMA dampers.

The total dissipation energy shows that the A-Steel and AP-Steel dampers dissipate more energy in comparison to the A-SMA and AP-SMA dampers, while the dissipation energy in the AF-SMA and APF-SMA dampers is more than that of the AF-Steel and APF-Steel. This energy dissipation in the APF-SMA damper is about 25% more than that of the APF-Steel damper (see Figs. 22 and 23). Furthermore, the energy ratio (*ER*) shows that the energy dissipation in the axial SMA dampers is about 42%, indicating that the energy dissipation of the SMA plates is more than that of the friction devices. But this ratio is approximately 73% and 95% in the AF-Steel and APF-Steel dampers, respectively, which indicates the dissipation energy in the steel plates is close to that of the friction devices. Therefore, the energy dissipation efficiency of the SMA plates is more than that of the steel plates in this damper.

6. Conclusions

This paper presents a recentering axial damper equipped with SMA plates, friction devices, and polyurethane springs. This damper can be employed in different kinds of bracing systems. To evaluate the effect of each component in the damper, the behavior of the damper was analyzed in the absence of each component, individually. Also, the SMA plates were replaced by steel plates to investigate the recentering and energy dissipation capabilities. All eight models were simulated on the ABAQUS platform and the results compared together. The results are as follows:

- The obtained results illustrated that the ABAQUS simulation is trustworthy and could represent the behavior of each component. The SMA plates played the role of a damper and recentering device. Furthermore, the friction devices worked as a friction damper and dissipated much energy. Also, the polyurethane springs increased the ultimate capacity of the damper.
- The proposed axial damper is very simple and does not need complex technology to produce and assemble. Also, this damper is a kind of rapid repair system which decreases the repairing costs after an earthquake event.
- The recentering SMA dampers dissipated a significant amount of energy such that the total dissipation energy in the APF-SMA damper is about 25% larger than that of the APF-Steel damper.
- The effect of the SMA plates on dissipating energy was more than that of the steel plates at the same displacement.
- The SMA recentering dampers could restore all the residual displacements while there is a lot of residual displacement upon unloading in axial steel dampers, which causes severe structural damages during strong earthquakes.
- The best case was the APF-SMA damper with maximum capacity, maximum energy dissipation, and very small residual displacement of about 0.43 mm with a 94% recentering ratio. This demonstrates that the combination of all components produces better performance.
- The axial steel dampers could not increase the dissipation energy even though the steel plates have

a rectangular shaped behavior overall, and the recentering ratio in all cases was less than 10%.

- Further research, including an experimental test, would be required to determine the real behavior of the proposed damper.
- For further investigation, the plan is to conduct an experimental test related to this damper in the near future.

Acknowledgments

This research was supported by Basic Science Research Program through the National Research Foundation of Korea (NRF) funded by the Ministry of Science, ICT & Future Planning (2017R1A2B2010120).

References

Alam, M.S., Youssef, M.A. and Nehdi, M. (2007), "Utilizing shape memory alloys to enhance the performance and safety of civil infrastructure: a review", *Can. J. Civ. Eng.*, **34**(9), 1075-1086.

Auricchio, F. and Sacco, E. (1997), "A one-dimensional model for superelastic shape-memory alloys with different elastic properties between austenite and martensite", *Int. J. Non. Linear. Mech.*, **32**(6), 1101-1114. https://doi.org/10.1016/S0020-7462(96)00130-8

Azariani, H.R., Reza Esfahani, M. and Shariatmadar, H. (2018), "Behavior of exterior concrete beam-column joints reinforced with Shape Memory Alloy (SMA) bars", *Steel Compos. Struct., Int. J.*, **28**(1), 83-98. https://doi.org/10.12989/scs.2018.28.1.083

DesRoches, R., McCormick, J. and Delemont, M. (2004), "Cyclic properties of superelastic shape memory alloy wires and bars", *J. Struct. Eng.*, **130**(1), 38-46. https://doi.org/10.1061/(ASCE)0733-9445(2004)130:1(38)

Elbahy, Y.I. and Youssef, M.A. (2019), "Flexural behaviour of superelastic shape memory alloy reinforced concrete beams during loading and unloading stages", *Eng. Struct.*, **181**, 246-259. https://doi.org/10.1016/j.engstruct.2018.12.001

Fang, C., Zheng, Y., Chen, J., Yam, M.C.H. and Wang, W. (2019), "Superelastic NiTi SMA cables: Thermal-mechanical behavior, hysteretic modelling and seismic application", *Eng. Struct.*, **183**, 533-549. https://doi.org/10.1016/j.engstruct.2019.01.049

Farmani, M.A. and Ghassemieh, M. (2016), "Shape memory alloy-based moment connections with superior self-centering properties", *Smart Mater. Struct.*, **25**(7). https://doi.org/10.1088/0964-1726/25/7/075028

Farzampour, A. and Eatherton, M.R. (2019), "Yielding and lateral torsional buckling limit states for butterfly-shaped shear links", *Eng. Struct.*, **180**, 442-451. https://doi.org/10.1016/j.engstruct.2018.10.040

Gao, N., Jeon, J.S., Hodgson, D.E. and Desroches, R. (2016), "An innovative seismic bracing system based on a superelastic shape memory alloy ring", *Smart Mater. Struct.*, **25**(5). https://doi.org/10.1088/0964-1726/25/5/055030

Hu, J.W., Noh, M.H. and Ahn, J.H. (2018), "Experimental investigation on the behavior of bracing damper systems by utilizing metallic yielding and recentering material devices", *Adv. Mater. Sci. Eng.*, **2018**. https://doi.org/10.1155/2018/2813058

Kari, A., Ghassemieh, M. and Abolmaali, S.A. (2011), "A new dual bracing system for improving the seismic behavior of steel structures", *Smart Mater. Struct.*, **20**(12). https://doi.org/10.1088/0964-1726/20/12/125020

Lu, X., Dang, X., Qian, J., Zhou, Y. and Jiang, H. (2017), "Experimental study of self-centering shear walls with horizontal bottom slits", *J. Struct. Eng.*, **143**(3). https://doi.org/10.1061/(ASCE)ST.1943-541X.0001673

Mirtaheri, M., Amini, M. and Khorshidi, H. (2017), "Incremental dynamic analyses of concrete buildings reinforced with shape memory alloy", *Steel Compos. Struct., Int. J.*, **23**(1), 95-105. https://doi.org/10.12989/scs.2017.23.1.095

Mirzaeifar, R., DesRoches, R. and Yavari, A. (2011), "A combined analytical, numerical, and experimental study of shape-memory-alloy helical springs", *Int. J. Solids Struct.*, **48**(3), 611-624. https://doi.org/10.1016/j.ijsolstr.2010.10.026

Mirzai, N.M., Attarnejad, R. and Hu, J.W. (2018), "Enhancing the seismic performance of EBFs with vertical shear link using a new self-centering damper", *Ing. Sismica*, **35**(4), 57-76.

Moradi, S. and Alam, M.S. (2015), "Feasibility study of utilizing superelastic shape memory alloy plates in steel beam-column connections for improved seismic performance", *J. Intell. Mater. Syst. Struct.*, **26**(4), 463-475. https://doi.org/10.1177/1045389X14529032

Ozbulut, O.E. and Hurlebaus, S. (2011), "Seismic assessment of bridge structures isolated by a shape memory alloy/rubber-based isolation system", *Smart Mater. Struct.*, **20**(1). https://doi.org/10.1088/0964-1726/20/1/015003

Pan, S., Hu, M., Zhang, X., Hui, H. and Wang, S. (2019), "A new near-surface-mounted anchorage system of shape memory alloys for local strengthening", *Smart Mater. Struct.*, **28**(2). https://doi.org/10.1088/1361-665X/aaf24e

Preciado, A., Ramírez-Gaytan, A., Gutierrez, N., Vargas, D., Falcon, J.M. and Ochoa, G. (2018), "Nonlinear earthquake capacity of slender old masonry structures prestressed with steel, FRP and NiTi SMA tendons", *Steel Compos. Struct.*, **26**(2), 213-226. https://doi.org/10.12989/scs.2018.26.2.213

Seo, J., Kim, Y.C. and Hu, J.W. (2015), "Pilot study for investigating the cyclic behavior of slit damper systems with recentering shape memory alloy (SMA) bending bars used for seismic restrainers", *Appl. Sci. (Switzerland)*, **5**(3), 187-208. https://doi.org/10.3390/app5030187

Silwal, B., Huang, Q., Ozbulut, O.E. and Dyanati, M. (2018), "Comparative seismic fragility estimates of steel moment frame buildings with or without superelastic viscous dampers", *J. Intell. Mater. Syst. Struct.*, **29**(18), 3598-3613. https://doi.org/10.1177/1045389X18798936

Speicher, M.S., DesRoches, R. and Leon, R.T. (2011), "Experimental results of a NiTi shape memory alloy (SMA)-based recentering beam-column connection", *Eng. Struct.*, **33**(9), 2448-2457. https://doi.org/10.1016/j.engstruct.2011.04.018

Speicher, M.S., DesRoches, R. and Leon, R.T. (2017), "Investigation of an articulated quadrilateral bracing system utilizing shape memory alloys", *J. Constr. Steel Res.*, **130**, 65-78. https://doi.org/10.1016/j.jcsr.2016.11.022

Sultana, P. and Youssef, M.A. (2016), "Seismic performance of steel moment resisting frames utilizing superelastic shape memory alloys", *J. Constr. Steel Res.*, **125**, 239-251. https://doi.org/10.1016/j.jcsr.2016.06.019

Wang, B., Zhu, S., Qiu, C.X. and Jin, H. (2019), "High-performance self-centering steel columns with shape memory alloy bolts: Design procedure and experimental evaluation", *Eng. Struct.*, **182**, 446-458. https://doi.org/10.1016/j.engstruct.2018.12.077

Xu, X., Tu, J., Cheng, G., Zheng, J. and Luo, Y. (2019), "Experimental study on self-centering link beams using post-tensioned steel-SMA composite tendons", *J. Constr. Steel Res.*, **155**, 121-128. https://doi.org/10.1016/j.jcsr.2018.12.026

Zahrai, S.M. (2015), "Cyclic testing of chevron braced steel frames with IPE shear panels", *Steel Compos. Struct., Int. J.*, **19**(5), 1167-1184. https://doi.org/10.12989/scs.2015.19.5.1167

Zahrai, S.M., Moradi, A. and Moradi, M. (2015), "Using friction dampers in retrofitting a steel structure with masonry infill panels", *Steel Compos. Struct., Int. J.*, **19**(2), 309-325. https://doi.org/10.12989/scs.2015.19.2.309

Zareie, S., Mirzai, N.M., Alam, M.S. and Seethlaer, R.J. (2017), "A dynamic analysis of a novel shape memory alloy-based bracing system", *Proceedings of the 6th International Conference on Engineering Mechanics and Materials*, Vancouver, Canada.

Zareie, S., Alam, M.S. and Seethlaer, R.J. (2019a), "A shape memory alloy-magnetorheological fluid core bracing system for civil engineering applications: feasibility study", *Proceedings of the 7th International Specialty Conference on Engineering Mechanics and Materials*, Laval, Canada.

Zareie, S., Alam, M.S., Seethlaer, R.J. and Zabihollah, A. (2019b), "Effect of shape memory alloy-magnetorheological fluid-based structural control system on the marine structure using nonlinear time-history analysis", *Appl. Ocean Res.* [In press] https://doi.org/10.1016/j.apor.2019.05.021

Zeynali, K., Saeed Monir, H., Mirzai, N.M. and Hu, J.W. (2018), "Experimental and numerical investigation of lead-rubber dampers in chevron concentrically braced frames", *Arch. Civ. Mech. Eng.*, **18**(1), 162-178. https://doi.org/10.1016/j.acme.2017.06.004

Zheng, Y. and Dong, Y. (2019), "Performance-based assessment of bridges with steel-SMA reinforced piers in a life-cycle context by numerical approach", *Bull. Earthq. Eng.*, **17**(3), 1667-1688. https://doi.org/10.1007/s10518-018-0510-x

BU